

Blindly Factorizing 21 Quantumly

Aritra Das^{1,2,*} and Barry C. Sanders^{1,†}

¹*Institute for Quantum Science and Technology, University of Calgary, Alberta T2N 1N4, Canada.*

²*Centre for Quantum Computation and Communication Technology,
Department of Quantum Science, Australian National University, ACT 2601, Australia.*

(Dated: July 20, 2022)

We develop a classically verifiable scheme for blindly factorizing the semiprime 21 quantumly for a classical client who does not trust the remote quantum servers. Our scheme advances state of the art, which achieves blind factorization of 15 quantumly, by increasing the problem to factorizing the next semiprime, choosing a harder base, executing a non-Clifford gate, and showing that the security check for 15 also works for 21. Our algorithmic approach to incorporating non-Clifford operations sets the stage for scaling blind quantum factorization, whereas our five-EPR-pair scheme motivates a photonic experiment that supplants current demonstrations of blind factorization.

I. INTRODUCTION

Nowadays commercial quantum computers, which strive for near-term intermediate-scale quantum advantages [1, 2], are accessed by the cloud [3] raising the problem of a client Clara (C) not trusting the remote server(s). Risk mitigation strategies include blind quantum computing (BQC) for weakly quantum clients (using either single-server prepare-and-send or receive-and-measure protocols) [4–9] and for purely classical clients (using multi-server entanglement-based protocols) [9–11] and quantum homomorphic encryption [12–15] whereby C delegates quantum computation to one or more remote servers, who are denied key information about the computation [6]. Building on successful experimental factorization of the odd semiprime (odd integer $N = pq$ for $p, q \in \mathbb{P}$ and $p \neq q$) $N = 15$ [10], we devise a protocol for C to delegate secure factorization of $N = 21$ [16] to two remote quantum servers called Alice (A) & Bob (B).

Our approach extends the BQC factorization of 15 in two ways [10]. First we increase N from 15 to the next odd semiprime number 21. Second, we choose a harder base a [17] for modular exponentiation (modexp) $f(x) := a^x \bmod N$ (where $\gcd(a, N) = 1$ with \gcd denoting greatest common divisor). The period r of $f(x)$ yields a solution $p = \gcd(a^{r/2} + 1, N)$ when the following two conditions are simultaneously met: (i) either r is even, or r is odd and a is a perfect square, and (ii) $a^{r/2} \not\equiv -1 \bmod N$. Period finding is sped up subexponentially by quantum computing [18]. For $N = 15$ with $a = 11$, $r = 2$ was achieved experimentally [10]; in contrast, we treat the hard case $N = 21$ with $a = 4$, for which $r = 3$. This harder a requires incorporating a non-Clifford operator, for which we employ the controlled-controlled-not (C²NOT or Toffoli) gate [19].

The remainder of our paper is organised as follows: In Sec. II, we summarily recall some relevant prerequisites

to our work and point to comprehensive resources on key topics. In Sec. III, we describe our methodology to construct a blind quantum factorization scheme for given N and a . In Sec. IV we present a formal algorithm, along with a function library, to design blind quantum factorization circuits for arbitrary N and a and also present the resulting circuits for two cases of $N = 21, a = 4$. We finish with a discussion on the significance of our results in Sec. V and a conclusion in Sec. VI.

II. BACKGROUND

In this section we briefly review the state-of-the-art in BQC, blind quantum factorization, and some other key concepts that are fundamental to our work. BQC is a quantum cryptographic protocol that allows clients with limited or no quantum hardware to outsource a computation to remote quantum server(s) without revealing information about the computation itself to the server(s) [5]. Several BQC protocols have already been developed and demonstrated for weakly quantum clients [4–7], but a purely classical client communicating only classically with a single quantum server might not be able to achieve secure BQC [20]. Nevertheless, this obstacle is overcome if multiple servers sharing non-local resources are employed [21]. A brief overview of verifiable BQC can be found in Ref. [9].

Secure BQC for completely classical clients, thus, warrants the remote and classical leveraging of quantum-advantageous algorithms, like Shor’s factorization [18] or Grover’s search [22], which serve as prime candidates for delegation [8, 10]. Delegated Shor’s factorization is known to be feasible in the measurement-based quantum computation model [5] and has been demonstrated experimentally for $N = 15$ in the quantum circuit model [10]. The approach in both these works comprises C delegating the quantum period-finding subroutine, which computes the period $r > 1$ of $f(x)$ for a given odd semiprime $N = pq$ with unknown p & q , of Shor’s algorithm to remote server(s). From the outputs returned by the servers to her, C classically computes the factors

* aritra.das@anu.edu.au

† sandersb@ucalgary.ca

as

$$p, q = \gcd(a^{r/2} \pm 1, N). \quad (1)$$

A proof-of-principle implementation of BQC for a completely classical client has been demonstrated in Ref. [10], wherein Shor’s algorithm [18] is executed for factorizing $N = 15$ using verifiable BQC based on the RUV protocol [21]. This blind quantum factorization was performed for the choice of base $a = 11$, which results in $r = 2$, thus making the experimental demonstration sufficiently challenging for a proof-of-concept but not as realistic as, for example, the case $a = 7$ and $r = 4$ would be. This is because $r = 2$ implies that the quantum period-finding circuit has reduced to a classical coin-toss experiment [23]—an anomaly that can be rationalised as the choice of base $a = 11$ (implicitly) assuming pre-knowledge of the factors [23].

A pre-knowledgeless factorization scheme would have to choose a random base a from some set of allowed bases. Without any prior ansatz, such a choice would yield a hard base with high probability; a hard base implies a period $r > 2$ and a period-finding circuit requiring the multi-qubit Toffoli gate, which is a non-Clifford operator. Introducing a non-Clifford operator brings the quantum resource called “magic” into play [24]. “Magic” enables quantum circuits to violate conditions for efficient classical simulatability [25, 26] so its inclusion is important for scaling considerations concerning BQC factorization’s quantum advantage. To this end, we now succinctly summarize the Clifford hierarchy of unitary operators.

The n -qubit Pauli group is

$$\mathcal{C}_n^{(1)} := \{\pm 1, \pm i\} \times \{I, X, Y, Z\}^{\otimes n}, \quad (2)$$

qubits being two-level systems spanned by logical states $|0\rangle, |1\rangle \in \mathcal{H}_2$, and \mathcal{H}_d a d -dimensional Hilbert space. Logical states are Z -eigenstates and comprise our computational basis, and

$$X, Y, Z \in \mathcal{U}(\mathcal{H}_2) \quad (3)$$

are the single-qubit Pauli operators, with $\mathcal{U}(\mathcal{H}_d)$ the group of unitary operators on \mathcal{H}_d . The n -qubit Clifford group $\mathcal{C}_n^{(2)}$ is the normalizer of the Pauli group, i.e.,

$$\mathcal{C}_n^{(2)} := \{u \in \mathcal{U}(\mathcal{H}_{2^n}); u \mathcal{C}_n^{(1)} u^\dagger \subseteq \mathcal{C}_n^{(1)}\}. \quad (4)$$

This group is generated by the Hadamard, phase (phase-shift by $\pi/2$) and controlled-not (CNOT) gates.

The Pauli and Clifford groups constitute the first two levels of the Clifford hierarchy, and the subsequent levels $\mathcal{C}_n^{(k>2)}$ are defined recursively by [27]

$$\mathcal{C}_n^{(k)} := \{u \in \mathcal{U}(\mathcal{H}_{2^n}); u \mathcal{C}_n^{(1)} u^\dagger \subseteq \mathcal{C}_n^{(k-1)}\}. \quad (5)$$

Conjugation with $\mathcal{C}_n^{(2)}$ maps $\mathcal{C}_n^{(1)}$ into itself, so Clifford operators can be blindly delegated using one-time Pauli pads [4]. However, $\mathcal{C}_n^{(2)}$ does not constitute a universal

gate-set. Moreover, stabilizer quantum circuits, which comprise only Clifford operators and computational basis measurements (corresponding to a projective-valued measure $|\epsilon\rangle\langle\epsilon|$ for $|\epsilon\rangle$ a computational basis state) [28], can be simulated efficiently (polynomial-time) classically [25, 26]. The experimental blind quantum factorization of 15 requires only a stabilizer circuit in its simplest form [10].

In contrast, the C^2NOT gate along with $\mathcal{C}_n^{(2)}$ constitutes a universal gate-set [29, 30]. A circuit comprising both Clifford and C^2NOT gates also circumvents the simulatability theorem [25, 26]. However, the inclusion of “magic” entails significant resource costs [12, 19]. Importantly, for our protocol, only one of A & B needs “magic” whereas the other executes a stabilizer circuit, thereby simplifying the scheme for experimental realization.

III. APPROACH

In this section we explain our approach to solving the blind quantum factorization of 21. First we describe the setup for blind quantum factorization, namely the classical client, the bipartite quantum server and their collective resources. Next we describe our mathematical representation of the computation circuit \mathcal{C} to be delegated to the servers and \mathcal{C} ’s associated representations. Our scheme for blind quantum factorization relies upon computation by teleportation on maximally entangled states, as identified in [27]; in spirit, this is similar to the RUV protocol [21] but we highlight some important distinctions in Sec. V. Next we establish the mathematical backbone of our scheme—a procedure to obtain two blind circuits, one for each server, from the circuit the classical client wishes to execute—via Lemma 1 and Fact 1. We conclude this section by reviewing the full procedure to obtain the blind quantum circuits from the input quantum circuit.

Similar to the BQC factorization of 15, which we summarize in Fig. 1 [10], our scheme is based on the Reichardt-Unger-Vazirani (RUV) protocol [21]. The RUV protocol is a multi-round, two-server BQC scheme for a classical client (as single-server BQC is not secure for classical clients [20, 31]). In each round of our protocol, servers A & B receive n copies of the entangled two-qubit pair $|\Phi\rangle := |00\rangle + |11\rangle \in \mathcal{H}_4$ (for $|00\rangle \equiv |0\rangle \otimes |0\rangle$, and implied normalization employed throughout) from a periodic source of entanglement, Deborah (D). Each server receives one qubit from each copy of $|\Phi\rangle$ and, thus, A & B collectively share the resource

$$|\Phi\rangle^{\otimes n} = (\mathbb{1} \otimes \mathbb{1} + X \otimes X)^{\otimes n} |00\rangle^{\otimes n} \in \mathcal{H}_{4^n} \quad (6)$$

but have no other means for communicating [21]. We index the $2n$ qubits in $|\Phi\rangle^{\otimes n}$ as shown in Fig. 1 for $n = 3$.

To delegate an n -qubit quantum circuit \mathcal{C} in the RUV protocol, C instructs each server to either compute, by executing a quantum circuit (\mathcal{A} for A, \mathcal{B} for B), or per-

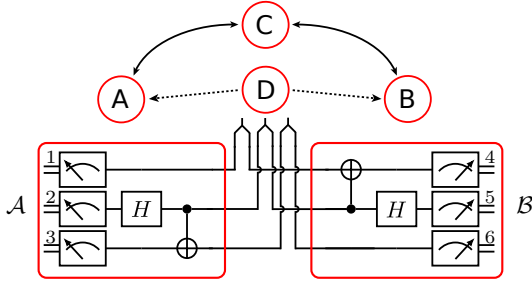


FIG. 1. BQC scheme for factorizing 15. Quantum servers A & B jointly compute circuits \mathcal{A} & \mathcal{B} (rounded rectangles), respectively, on state $|\Phi\rangle^{\otimes 3}$ supplied by entanglement source D, and report outcomes to classical client C. Each of \mathcal{A} & \mathcal{B} involves a CNOT and a Hadamard gate (H), and Z -basis measurements. Solid and dotted arrows represent classical and quantum communication, respectively, arrowheads indicate directionality, and numbers represent indices for qubits.

form the measurement part of a Clauser-Horne-Shimony-Holt (CHSH) test [32]. There are, thus, four distinct subprotocols: A & B could both compute (computational subprotocol), or both measure (CHSH subprotocol), or else one computes while the other measures (two tomography subprotocols) [21]. When both compute, A & B report to C their i^{th} Z -measurement outcomes

$$\{(a_i, b_i); a_i, b_i \in \{0, 1\}, i \in [n] := \{1, \dots, n\}\}. \quad (7)$$

From their combined outcomes, C recovers the output from \mathcal{C} whereas the output from either \mathcal{A} or \mathcal{B} alone yields no information about \mathcal{C} except depth, thereby blinding A & B.

Now we discuss the underlying primitive gates for \mathcal{C} over n qubits. Each computational cycle, with execution by circuit component \mathcal{C}_ν , allows one or more of the following primitive gates operating in parallel:

- (i) single-qubit Hadamard (H),
- (ii) single-qubit NOT (X),
- (iii) two-qubit controlled-rotation (CR^k), and
- (iv) multi-controlled NOT (C^lNOT , where $l \in [n-1]$ denotes the number of controls), also known as the multi-controlled Toffoli gate.

Our CR^k gates are restricted to rotations R^k : $0 \leq k < n$ that impart a phase of $\pi/2^k$ on $|1\rangle$ and zero phase on $|0\rangle$. Our choice of primitives is natural for Shor factorization [18], and these primitives are composites of the “standard set” of CNOT, H and the R^2 gate called T , as described in the Appendix A [23, 29, 33–35].

In Appendix B, we show that there are at most

$$\left(\frac{1133233}{8!} \right) n^{n/2} n! \quad (8)$$

allowed circuit components over n qubits, so we can label \mathcal{C}_ν by a bit string $\mathbf{B}(\mathcal{C}_\nu)$ with size at most

$$\left\lceil \log \left\{ \left(\frac{1133233}{8!} \right) n^{n/2} n! \right\} \right\rceil. \quad (9)$$

The depth d circuit \mathcal{C} is then a composition of d circuit components,

$$\mathcal{C} = \bigcirc_{\nu=1}^d \mathcal{C}_\nu := \mathcal{C}_d \circ \dots \circ \mathcal{C}_1, \quad (10)$$

where \mathcal{C}_ν is the circuit component for the ν^{th} computational cycle and \circ denotes composition. Correspondingly, \mathcal{C} is represented by the bit string

$$\mathbf{B}(\mathcal{C}) = \parallel_{\nu=1}^d \mathbf{B}(\mathcal{C}_\nu), \quad (11)$$

where \parallel denotes concatenation of bit strings. We also represent each circuit component \mathcal{C}_ν by unitary operator $G_\nu \in \mathcal{U}(\mathcal{H}_{2^n})$ and represent \mathcal{C} by unitary operator $G \in \mathcal{U}(\mathcal{H}_{2^n})$, so that

$$G = G_d G_{d-1} \dots G_1. \quad (12)$$

We now focus on RUV-based blind quantum factorization of odd semiprime N , wherein factorization circuit \mathcal{C} acts on two computational registers of sizes t and L [18, 36]. Thus, now $n = t + L$, and the registers are collectively initialized to $|0\rangle^{\otimes n}$. For uncompiled factorization circuits, $t \geq 2\lceil \log N \rceil + 1$ and $L \geq \lceil \log N \rceil$, but we employ compilation so these bounds do not apply [17]. To convert \mathcal{C} into blind circuits \mathcal{A} & \mathcal{B} , we employ a two-step procedure: first we partition \mathcal{C} into a first-stage circuit $\mathcal{C}_<$ and a second-stage circuit $\mathcal{C}_>$; then we convert the sequential computation $\mathcal{C}_> \circ \mathcal{C}_<$ into a bipartite computation $\mathcal{A} \otimes \mathcal{B}$ on $|\Phi\rangle^{\otimes n}$.

In our scheme we require \mathcal{A} to be a stabilizer circuit, and \mathcal{B} to have the minimum possible d . Thus, before partitioning \mathcal{C} , we first minimize reduced depth $d_>$ (defined to be the number of cycles including the first non-Clifford cycle and then all subsequent cycles, whether Clifford or not) over all circuits that are permutations of the cycles of \mathcal{C} and are \mathcal{C} -equivalent (i.e., map input to the same output as \mathcal{C}). In case the minimum reduced depth $d_>^*$ is not achieved uniquely, we choose an optimal circuit \mathcal{C}^* . Then, $\mathcal{C}_<$ is the composition of the first $d - d_>^*$ cycles in \mathcal{C}^* and $\mathcal{C}_>$ is the composition of the last $d_>^*$ cycles in \mathcal{C}^* . Thus, for

$$\mathcal{C}^* = \bigcirc_{\nu=1}^d \mathcal{C}_\nu^*, \quad (13)$$

we partition as

$$\mathcal{C}_< := \bigcirc_{\nu=1}^{d-d_>^*} \mathcal{C}_\nu^* \quad \& \quad \mathcal{C}_> := \bigcirc_{\nu=d-d_>^*+1}^d \mathcal{C}_\nu^*, \quad (14)$$

so that

$$\mathcal{C}^* = \mathcal{C}_> \circ \mathcal{C}_<. \quad (15)$$

The bit strings $\mathbf{B}(\mathcal{C}_<)$ & $\mathbf{B}(\mathcal{C}_>)$ representing $\mathcal{C}_<$ & $\mathcal{C}_>$, respectively, are determined by first permuting the component bit strings of $\mathbf{B}(\mathcal{C})$ and then partitioning into $\mathbf{B}(\mathcal{C}_<)\parallel\mathbf{B}(\mathcal{C}_>)$ following Eq. (14); we denote this operation by the bit-string function PART.

To establish the second step in our procedure, we first introduce some notation, prove a lemma and state a fact.

Below we denote transposition in the computational basis by $^\top$. For $x = (x_n \cdots x_1) \in \{0, 1\}^n$, we define

$$X^x := X_n^{x_n} \otimes \cdots \otimes X_1^{x_1} \in \mathcal{U}(\mathcal{H}_{2^n}), \quad (16)$$

where the subscripts below X indicate the index of the qubit being targeted. Thus, a computational basis state is

$$|x\rangle = X^x |0\rangle^{\otimes n} \in \mathcal{H}_{2^n}. \quad (17)$$

Lemma 1. *For any $x \in \{0, 1\}^n$ and unitary operators $G_<, G_>, G_A, G_B \in \mathcal{U}(\mathcal{H}_{2^n})$, the mapping*

$$X^x G_<^\top \mapsto G_A, \quad X^x G_> \mapsto G_B \quad (18)$$

leads to the equality

$$X^x G_> G_< X^x |0\rangle^{\otimes n} = \left(\langle 0|^{\otimes n} G_A \otimes G_B \right) |\Phi\rangle^{\otimes n}. \quad (19)$$

Proof. From the ‘‘ricochet’’ property [37],

$$\begin{aligned} & (\langle 0|^{\otimes n} \langle 0|^{\otimes n} G_A \otimes G_B) (\mathbb{1} \otimes \mathbb{1} + X \otimes X)^{\otimes n} \\ &= \left[\mathbb{1} \otimes \left(G_B G_A^\top |0\rangle^{\otimes n} \langle 0|^{\otimes n} \right) \right] (\mathbb{1} \otimes \mathbb{1} + X \otimes X)^{\otimes n}, \end{aligned} \quad (20)$$

so assign $G_A \leftarrow X^x G_<^\top$ and $G_B \leftarrow X^x G_>$. \square

Fact 1. As each of our primitive gates admits a symmetric matrix representation in the computational basis, the operator $G_<^\top$ represents a circuit $\mathcal{C}_<^\top$ that consists of the components of $\mathcal{C}_<$ executed in reverse order, i.e.,

$$\mathcal{C}_<^\top := \bigcirc_{\nu=d-d^*}^1 \mathcal{C}_\nu^*. \quad (21)$$

We denote the operation of obtaining $\mathcal{B}(\mathcal{C}_<^\top)$ by reversing the order of components in $\mathcal{B}(\mathcal{C}_<)$ by the bit-string function REV.

We now explain how we use Lemma 1 and Fact 1 to convert $\mathcal{C}_> \circ \mathcal{C}_<$ into $\mathcal{A} \otimes \mathcal{B}$. Let $G_<, G_>, G_A$ and G_B be unitary operators representing $\mathcal{C}_<, \mathcal{C}_>, \mathcal{A}$ and \mathcal{B} , respectively, so that Map (18) implies

$$\mathcal{A} = X^x \circ \mathcal{C}_<^\top \quad \& \quad \mathcal{B} = X^x \circ \mathcal{C}_>. \quad (22)$$

Also, consider any $x \in \{0, 1\}^{t+L}$ with $x_i = 0$ for all $i \in [t]$. Then,

$$X^x G_> G_< X^x = G_> G_< = G, \quad (23)$$

because the second register of \mathcal{C} is operated on by only \mathcal{C}^l NOTs [18], and Eq. (19) simplifies to

$$G |0\rangle^{\otimes n} = \langle x | G_<^\top \otimes X^x G_> | \Phi \rangle^{\otimes n}. \quad (24)$$

As the output from only the first register of \mathcal{C}^* is used to compute r [18], the X^x in Eq. (24) can be ignored. Finally, we have

$$\mathcal{A} = \mathcal{C}_<^\top \quad \& \quad \mathcal{B} = \mathcal{C}_>, \quad (25)$$

and B’s outcomes $\{b_i; i \in [t]\}$ are identical to the output from the first register of \mathcal{C} whenever A reports $a_i = 0$ for all $i \in [t]$. This completes our description of the procedure to obtain \mathcal{A} & \mathcal{B} from \mathcal{C} .

IV. RESULTS

In this section we present our results, which are two-fold. Firstly, we present a scalable algorithm to design circuits \mathcal{A} & \mathcal{B} for blind-quantumly factorizing arbitrary odd semiprime N using arbitrary base a . Secondly, we present the outputs of this algorithm, i.e., the factorization circuits \mathcal{A} & \mathcal{B} , along with the rest of the blind factorization scheme, for two cases corresponding to $N = 21$ and $a = 4$. Our algorithm requires certain standard functions so we start by specifying a function library, though we don’t reproduce the corresponding algorithms here as they are standard in literature.

We now introduce our concept for the function library FUNCLIB for designing circuits \mathcal{A} & \mathcal{B} . FUNCLIB comprises four functions, with two of them (PART & REV) already discussed and the other two well established in literature on factorization [17, 18, 38]. The integer function

$$\text{MAXDEP}(N, a) = 96 \lceil \log a \rceil \lceil \log N \rceil^2 \quad (26)$$

yields an upper bound on factorization-circuit depth, given N and a , based on complexity arguments for scaling modular exponentiation [38]. The bit-string function SHORCIR returns a bit string representing the compiled factorization circuit, given N, a, t and n [17, 18]. Our procedure for designing circuits \mathcal{A} & \mathcal{B} is described in Alg. 1, where we employ ‘type’ notation USINT for nonnegative integers and BIN for bit strings (with $[]$ denoting array size).

Algorithm 1 Parallelizing Factorization

Input:

USINT NUM	$\triangleright N = pq, p \neq q, p, q \in \mathbb{P} \setminus \{2\}$
USINT BASE	\triangleright Base $a: a < N, \gcd(a, N) = 1$
USINT SIZ1	\triangleright First-register size of Shor circuit
USINT SIZ2	\triangleright Second-register size of Shor circuit

Output:

BIN[] CIRCDISA, CIRDES B
1: procedure CIRDESIGN(NUM, BASE, SIZ1, SIZ2)
2: Import FUNCLIB \triangleright For functions
3: USINT DEPTH, SIZECOM, SIZCIR
4: DEPTH \leftarrow MAXDEP(NUM, BASE) \triangleright Eq. (26)
5: SIZ2 \leftarrow SIZ1 + SIZ2 \triangleright Replace by total register size
6: SIZECOM $\leftarrow \lceil \log(\frac{133233}{8!} * \text{SIZ2} * * \frac{\text{SIZ2}}{2} * \text{SIZ2}!) \rceil$
7: SIZCIR \leftarrow SIZECOM * DEPTH \triangleright Space-time product
8: BIN[SIZCIR] CIRDES, CIRDES L, CIRDES G, CIRDES A, CIRDES B
9: CIRDES \leftarrow SHORCIR(NUM, BASE, SIZ1, SIZ2)
10: CIRDES L CIRDES G \leftarrow PART(CIRDES) \triangleright Optimal partition
11: CIRDES A \leftarrow REV(CIRDES L) \triangleright Reverse order
12: CIRDES B \leftarrow CIRDES G
13: end procedure

Next we describe the computational subprotocol for our scheme. Prior to executing the subprotocol, C runs Alg. 1 to design \mathcal{A} & \mathcal{B} and sends the output bit strings to the servers. Then, in every instance of the subprotocol,

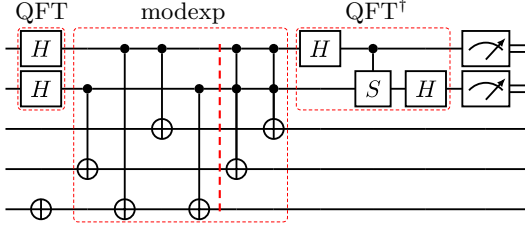


FIG. 2. Optimally permuted \mathcal{C}^* for $N = 21, a = 4, t = 2$ and $L = 3$. Unlabeled input states are $|0\rangle$ and measurements are in the Z basis. Quantum Fourier transform (QFT) is performed using Hadamard (H) gates, modexp using CNOT and C^2 NOT gates, and inverse QFT (QFT^\dagger) using a controlled-phase gate (S) and Hadamard gates. The vertical dashed line (red) indicates the optimal partition of the circuit.

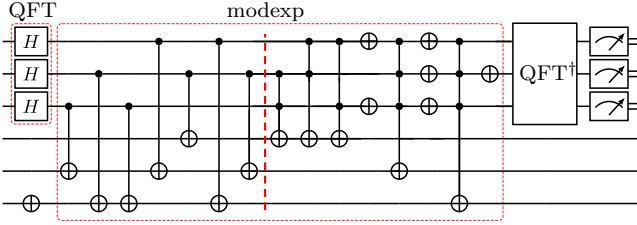


FIG. 3. Optimally permuted \mathcal{C}^* for $N = 21, a = 4, t = 3$ and $L = 3$. Unlabeled input states are $|0\rangle$ and measurements are in the Z basis. QFT is performed using Hadamard (H) gates, modexp using NOT, CNOT, C^2 NOT, and C^3 NOT gates. The inverse QFT (QFT^\dagger) is abridged as a 3-qubit gate for readability. The vertical dashed line (red) indicates the optimal partition of the circuit.

\mathcal{C} instructs \mathcal{A} & \mathcal{B} to execute their circuits and report measurement outcomes. If $a_i = 0$ for all $i \in [t]$, which occurs with probability 2^{-t} , \mathcal{C} computes a candidate for r by classically processing $\{b_i; i \in [t]\}$. For completeness, we describe this classical processing in Appendix C. The exponentially small probability could be improved by instructing \mathcal{B} to Pauli-correct before computing, but doing so blindly would entail higher space requirements [21, 27]; in this work we instead focus on N with t sufficiently small for 2^{-t} to be a feasible probability.

This concludes our discussion of the computation sub-protocol, whereas the three other RUV subprotocols are standard so we describe them in Appendix D. In our full multi-round protocol for blind quantum factorization (summarized in Appendix D), \mathcal{C} runs one of the four sub-protocols at random, interacting with the servers as required, until the correct r is found. Although tomographic verification via the stabilizer framework [10, 21] is inapplicable here due to our inclusion of non-Clifford operators [39, 40], \mathcal{C} can classically verify r in $\text{polylog } N$ time by checking $\text{gcd}(p, N) = p \in \mathbb{P}$ [9].

We now present circuits \mathcal{C}^* , \mathcal{A} and \mathcal{B} specifically for $N = 21$ and $a = 4$ with two cases considered, namely $t = 2$ and $t = 3$, both with $L = 3$. The five-qubit ($t = 2$) and six-qubit ($t = 3$) optimally permuted

circuits \mathcal{C}^* are shown in Figs. 2 and 3, respectively, where a vertical dashed line indicates the partition into a first and a second stage. For both cases, the output from the first register of \mathcal{C}^* is shown in Fig. 5 in Appendix C. For $t = 2$, the blind circuits \mathcal{A} & \mathcal{B} are shown in Fig. 4. For $t = 3$, we do not show \mathcal{A} & \mathcal{B} explicitly as they could be similarly obtained from \mathcal{C}^* in Fig. 3: \mathcal{A} is the first stage performed in reverse order whereas \mathcal{B} is the second stage. Both \mathcal{A} & \mathcal{B} terminate with Z measurements of all qubits.

V. DISCUSSION

In this section, we discuss the significance some implications of our results. Our Alg. 1 designs scalable blind quantum factorization circuits for arbitrary N and a , with expected number of runs growing as 2^t (note that we use compiled circuits, so t is not restricted by the $2\lceil \log N \rceil + 1$ bound). Alg. 1, via PART, also ensures that \mathcal{A} is always a stabilizer circuit, and thus not resource-intensive to implement. Moreover, \mathcal{A} can be implemented fault-tolerantly straightforwardly [27] and affords complete tomographic verification via just CHSH measurements [21].

On the other hand, we expect \mathcal{B} to include non-Clifford operations and be resource intensive (potentially experimentally infeasible at present). This can also be seen in the circuits \mathcal{C}^* , \mathcal{A} and \mathcal{B} for $t \in \{2, 3\}$. For $t = 2$, \mathcal{C}^* has $d = 8$, $d_{\geq}^* = 5$ and incorporates three non-Clifford gates (one CR^1 and two C^2 NOTs); \mathcal{A} & \mathcal{B} thus have depths of three & five, respectively. For $t = 3$, \mathcal{C}^* has $d = 17$, $d_{\geq}^* = 13$ and incorporates eight non-Clifford gates (one CR^2 , two CR^1 s, three C^2 NOTs and two C^3 NOTs); \mathcal{A} & \mathcal{B} thus have depths of four & thirteen, respectively. In both cases, \mathcal{A} is conveniently a stabilizer circuit whereas \mathcal{B} incorporates all non-Clifford gates in \mathcal{C}^* .

For $t = 2$, despite following Shor's algorithm [16], \mathcal{C}^* never yields the correct period due to insufficient space in the first register; hence, \mathcal{A} & \mathcal{B} fail to factorize 21. However, the output from \mathcal{C}^* is sufficient to establish a proof-of-concept as in Ref. [16]. Further, photonic implementations of \mathcal{A} & \mathcal{B} , which entail scaling up from one C^2 NOT to two [41] and from three EPR pairs to five [10], are more feasible in this case compared to $t = 3$. For $t = 3$, \mathcal{C}^* delivers the correct period with probability 0.47 so \mathcal{A} & \mathcal{B} succeed in factorizing with probability 0.058, but \mathcal{B} requires significant resources.

Another advantage of our blind quantum factorization scheme is the low qubit count required to factorize N . Our scheme requires, at worst, $O(\log N)$ qubits to guarantee factorization compared to the $O((\log N)^2)$ qubits a literal adaptation of the RUV protocol to quantum factorization would require. Finally, we remedy RUV's open problem of tomographic verifiability of non-Clifford computations in the context of factorization by declaring \mathcal{B} to be dishonest if \mathcal{C} finds \mathcal{A} honest (which requires only

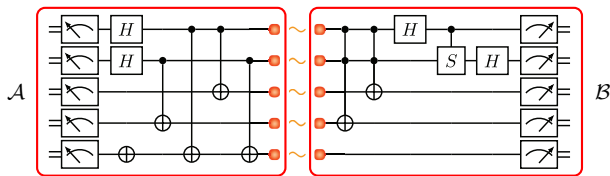


FIG. 4. Blind circuits \mathcal{A} & \mathcal{B} for $N = 21, a = 4, t = 2$ and $L = 3$. \mathcal{A} & \mathcal{B} (rounded rectangles) each act on input registers initialized to one half of the bipartite state $|\Phi\rangle^{\otimes 5}$ (red dots). \mathcal{A} comprises NOT, CNOT, and Hadamard (H) gates whereas \mathcal{B} comprises C^2 NOT, controlled-phase (S) and Hadamard gates. All measurements are in the Z basis.

CHSH measurements) but still does not receive the correct period (which can be checked efficiently classically) from B.

VI. CONCLUSIONS

Here we have developed a BQC scheme for factorizing 21. Our multi-round protocol is accessible to a classical client, who communicates with two remote quantum

servers. The servers send the client Z -measurement results for each round. By processing these data, the client determines candidates for factors of 21 or verifies honesty of the servers, all while concealing the actual task. Our choice of hard a implies that servers employ non-Clifford gates, which is a non-trivial requirement unseen for $N = 15$ [10]; our non-Clifford analysis establishes a foundation for future BQC factorization protocols. Finally, our protocol for $t = 2$ motivates a challenging but feasible photonic experiment that would set a milestone towards secure quantum computation for classical clients.

ACKNOWLEDGMENTS

Aritra Das thanks and acknowledges financial support from the Shastri Indo-Canadian Institute through their Shastri Research Student Fellowship program and from the Australian Research Council Centre of Excellence CE170100012. Aritra Das is also grateful to the Indian Institute of Technology Kanpur, where a majority of this work was undertaken. Finally, Aritra Das and Barry C. Sanders acknowledge the traditional owners of the land on which this work was undertaken at the University of Calgary: the Treaty 7 First Nations.

-
- [1] J. Preskill, [Quantum](#) **2**, 79 (2018).
 - [2] J. Preskill, arXiv: Quantum Physics (2012).
 - [3] S. J. Devitt, [Phys. Rev. A](#) **94**, 032329 (2016).
 - [4] A. M. Childs, [Quantum Inf. Comput.](#) **5**, 456 (2005).
 - [5] A. Broadbent, J. Fitzsimons, and E. Kashefi, in *Proceedings of the 50th Annual IEEE Symposium on Foundations of Computer Science* (IEEE Computer Society, New York, 2009) pp. 517–526.
 - [6] J. F. Fitzsimons, [npj Quantum Inf.](#) **3**, 23 (2017).
 - [7] J. F. Fitzsimons and E. Kashefi, [Phys. Rev. A](#) **96**, 012303 (2017).
 - [8] S. Barz, E. Kashefi, A. Broadbent, J. F. Fitzsimons, A. Zeilinger, and P. Walther, [Science](#) **335**, 303 (2012).
 - [9] A. Gheorghiu, T. Kapourniotis, and E. Kashefi, [Theory Comput. Syst.](#) **63**, 715 (2019).
 - [10] H.-L. Huang, Q. Zhao, X. Ma, C. Liu, Z.-E. Su, X.-L. Wang, L. Li, N.-L. Liu, B. C. Sanders, C.-Y. Lu, and J.-W. Pan, [Phys. Rev. Lett.](#) **119**, 050503 (2017).
 - [11] A. Cojocaru, L. Colisson, E. Kashefi, and P. Wallden, [Cryptography](#) **5**, 3 (2021).
 - [12] A. Broadbent and S. Jeffery, in *Advances in Cryptology, Lecture Notes in Computer Science*, Vol. 9216 (Springer, Berlin, 2015) pp. 609–629.
 - [13] Y. Ouyang, S.-H. Tan, and J. F. Fitzsimons, [Phys. Rev. A](#) **98**, 042334 (2018).
 - [14] W. K. Tham, H. Ferretti, K. Bonsma-Fisher, A. Brodutch, B. C. Sanders, A. M. Steinberg, and S. Jeffery, [Phys. Rev. X](#) **10**, 011038 (2020).
 - [15] Y. Ouyang, S.-H. Tan, J. Fitzsimons, and P. P. Rohde, [Phys. Rev. Research](#) **2**, 013332 (2020).
 - [16] E. Martín-López, A. Laing, T. Lawson, R. Alvarez, X.-Q. Zhou, and J. L. O’Brien, [Nat. Photonics](#) **6**, 773 (2012).
 - [17] J. A. Smolin, G. Smith, and A. Vargo, [Nature \(London\)](#) **499**, 163 (2013).
 - [18] P. W. Shor, [SIAM J. Comput.](#) **26**, 1484 (1997).
 - [19] Y. Shi, [Quantum Inf. Comput.](#) **3**, 84 (2003).
 - [20] S. Aaronson, A. Cojocaru, A. Gheorghiu, and E. Kashefi, in *Proceedings of the 46th International Colloquium on Automata, Languages and Programming*, Leibniz International Proceedings in Informatics (LIPIcs), Vol. 132 (Schloss Dagstuhl–Leibniz-Zentrum für Informatik, Dagstuhl, Germany, 2019) pp. 6:1–6:13.
 - [21] B. W. Reichardt, F. Unger, and U. Vazirani, [Nature \(London\)](#) **496**, 456 (2013).
 - [22] L. K. Grover, [Phys. Rev. Lett.](#) **79**, 4709 (1997).
 - [23] V. V. Shende and I. L. Markov, [Quantum Inf. Comput.](#) **9**, 461 (2009).
 - [24] S. Bravyi and A. Kitaev, [Phys. Rev. A](#) **71**, 022316 (2005).
 - [25] D. Gottesman, in *Proceedings of the 22nd International Colloquium on Group Theoretical Methods in Physics* (International Press, Cambridge, 1999) pp. 32–43.
 - [26] S. Aaronson and D. Gottesman, [Phys. Rev. A](#) **70**, 052328 (2004).
 - [27] D. Gottesman and I. L. Chuang, [Nature \(London\)](#) **402**, 390 (1999).
 - [28] A. R. Calderbank, E. M. Rains, P. W. Shor, and N. J. A. Sloane, [Phys. Rev. Lett.](#) **78**, 405 (1997).
 - [29] P. Boykin, T. Mor, M. Pulver, V. Roychowdhury, and F. Vatan, [Inf. Process. Lett.](#) **75**, 101 (2000).
 - [30] T. Pillaha, N. Rengaswamy, O. Tirkkonen, and R. Calderbank, [Quantum](#) **4**, 370 (2020).
 - [31] T. Morimae and T. Koshiha, [Quantum Inf. Comput.](#) **19**, 214 (2019).

- [32] J. F. Clauser, M. A. Horne, A. Shimony, and R. A. Holt, *Phys. Rev. Lett.* **23**, 880 (1969).
- [33] A. Barenco, C. H. Bennett, R. Cleve, D. P. DiVincenzo, N. Margolus, P. Shor, T. Sleator, J. A. Smolin, and H. Weinfurter, *Phys. Rev. A* **52**, 3457 (1995).
- [34] D. Maslov, G. Dueck, and D. Miller, *IEEE Trans. Comput.-Aided Des. Integr. Circuits Syst.* **24**, 807 (2005).
- [35] D. Gosset, V. Kliuchnikov, M. Mosca, and V. Russo, *Quantum Inf. Comput.* **14**, 1261–1276 (2014).
- [36] M. A. Nielsen and I. L. Chuang, *Quantum Computation and Quantum Information*, 10th ed. (Cambridge University Press, Cambridge, 2010).
- [37] M. M. Wilde, *Quantum Information Theory*, 2nd ed. (Cambridge University Press, Cambridge, 2017).
- [38] D. Beckman, A. N. Chari, S. Devabhaktuni, and J. Preskill, *Phys. Rev. A* **54**, 1034 (1996).
- [39] B. W. Reichardt, F. Unger, and U. V. Vazirani, in *Proceedings of the 4th Innovations in Theoretical Computer Science* (Association for Computing Machinery, New York, 2013) pp. 321–322.
- [40] D. F. V. James, P. G. Kwiat, W. J. Munro, and A. G. White, *Phys. Rev. A* **64**, 052312 (2001).
- [41] B. P. Lanyon, T. J. Weinhold, N. K. Langford, M. Barbieri, D. F. V. James, A. Gilchrist, and A. G. White, *Phys. Rev. Lett.* **99**, 250505 (2007).

APPENDIX A: DECOMPOSITION OF PRIMITIVES INTO STANDARD SET

Our primitive gates are composites of the usual primitive set of CNOT, H and the R^2 gate called T , and we explain briefly how our gates decompose to this “standard set” [29]. A CR^k gate can be performed using two CNOTs and two R^{k+1} gates [33]. A C^l NOT (for $l \geq 3$) can be performed using $l-2$ “dirty” ancillae and $4l-8$ C^2 NOTs [33], or $l-2$ “clean” ancillae and $2l-3$ C^2 NOTs [34]. Here, “clean” ancillae are qubits initialised to some computational basis state $|x\rangle$, whereas “dirty” ancillae are in some unknown state in \mathcal{H}_2 to which they must be restored post-computation. Finally, each C^2 NOT requires seven T gates, two H gates, one R^1 gate and six CNOTs [23, 35].

APPENDIX B: SIZE OF BIT-STRING REPRESENTATION

Now we establish an upper bound on the size of a bit string $\mathbf{B}(\mathcal{C}_\nu)$ representing any circuit component \mathcal{C}_ν over n qubits. An upper bound on this size is given by $\lceil \log(s(n)) \rceil$, for $s(n)$ the number of distinct circuit components (including the identity component $1^{\otimes n}$) on n qubits. Correspondingly, we posit an upper bound on $s(n)$, from which the bound on size follows.

First consider the closely related quantity $s'(n)$, which is the number of distinct circuit components over n qubits, ignoring the argument k of the CR gates. Then,

for $n \geq 1$, we have the recurrence relation

$$s'(n) = 3s'(n-1) + 2(n-1)s'(n-2) + \sum_{j=0}^{n-2} \binom{n-1}{j} (n-j)s'(j). \quad (27)$$

Along with initial conditions $s'(0) = 1$ and $s'(n < 0) = 0$, Eq. (27) can be used to compute $s'(n)$ for any $n \geq 1$. Next we prove the bound

$$s'(n) < cn! \quad \forall n \in \mathbb{N}, \quad (28)$$

where c is some positive constant. Numerical evidence suggests $s'(n)/n!$ increases up to $n = 8$, and then decreases monotonically. Correspondingly, we choose

$$c := \max_{1 \leq n \leq 8} \frac{s'(n)}{n!} = \frac{1133233}{8!} \quad (29)$$

so that inequality (28) is satisfied for $n \in [8]$ trivially.

Next we show that inequality (28) holds for $n > 8$ by using strong induction on n with base case $n = 8$. In the inductive step, we prove that inequality (28) holds for $n > 8$ if it holds for all $j \in [n-1]$. From Eq. (27) we have

$$s'(n) \leq c \left[7(n-1)! + \sum_{j=0}^{n-3} \binom{n-1}{j} (n-j)j! \right]. \quad (30)$$

Using $\sum_{j=0}^{n-1} 1/j! < e$, we get

$$\sum_{j=0}^{n-1} \binom{n-1}{j} (n-j)j! < 2e(n-1)! \quad (31)$$

so that

$$s'(n) < c(4 + 2e)(n-1)! < cn!, \quad (32)$$

where this last inequality relies on $n > 8$.

Note that there are at most $\lfloor n/2 \rfloor$ CR gates in any n -qubit component and n choices of k ($0 \leq k < n$) for each CR gate. Thus,

$$s(n) \leq n^{n/2} s'(n) \leq cn^{n/2} n! \quad (33)$$

and the size of $\mathbf{B}(\mathcal{C}_\nu)$ is at most $\lceil \log(cn^{n/2} n!) \rceil$.

APPENDIX C: RECOVERING FACTORS FROM CIRCUIT OUTPUT

Here we briefly describe the classical post-processing procedure to obtain a candidate r , and thereby factors p and q , from the first-register output of a factorization circuit [18]. Given an output $y \in \{0, 1\}^t$ from the first register, the procedure involves calculating continued fraction convergents d/s for $y/2^t$ such that $s < N$ and $|d/s - y/2^t| < 1/2^{t+1}$. Then, s is a candidate for r

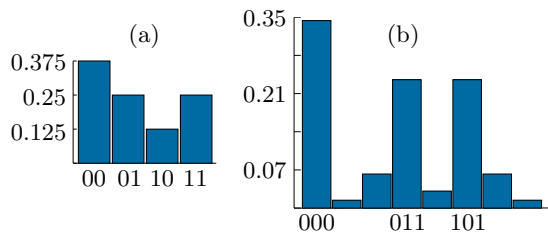


FIG. 5. Mean probabilities of measurement of the first register of \mathcal{C}^* for (a) $t = 2$ and (b) $t = 3$. The rightmost bit corresponds to the topmost qubit in Figs. 2 & 3.

and if $a^s = 1 \pmod{N}$ and if $a^{s/2} \neq -1 \pmod{N}$, s is the period r . Finally, the factors of N are calculated as $p, q = \gcd(a^{r/2} \pm 1, N)$.

For $N = 21$, we show the output from the first register of \mathcal{C}^* along with their measurement probabilities in Fig. 5(a) and (b) for the $t = 2$ and the $t = 3$ circuit, respectively. Post-processing each measurement outcome for $t = 2$, we find that the $t = 2$ circuit never yields the correct r . However, the correct period could be obtained via additional heuristic post-processing, which involves checking whether multiples of s or $s \pm 1, s \pm 2, \dots$ are the period. Moreover, the measurement outcomes in Fig. 5(a) have been experimentally verified [16]. In contrast, the $t = 3$ circuit yields the correct r for $y = 011$ and $y = 101$. Each of these two outcomes occurs with a probability of 0.235, so the $t = 3$ circuit succeeds in factorizing 21 with probability 0.47.

APPENDIX D: SUMMARY OF OVERALL PROTOCOL

In this section, we provide a summary of our protocol for blind quantum factorization, which comprises four subprotocols. We have already discussed the computational subprotocol in the main text, whereas our implementation of the three other subprotocols—the CHSH and both tomography subprotocols—is standard [10, 21]. Thus, we first briefly describe these three subprotocols, and then we outline the overall protocol for \mathcal{C} .

In the CHSH subprotocol, \mathcal{C} runs multiple rounds of the CHSH game between the servers [10, 32]. CHSH rigidity ensures that, if the servers win an optimal fraction of rounds, their shared resource is indeed $|\Phi\rangle$ and they have been honest in computational basis measurements [21, 39]. The two tomography subprotocols verify whether one server has computed correctly by collating the other server’s simultaneous X - or Z -basis measurement outcomes. Whereas such measurements are sufficient for state verification in the case $N = 15$ (due to only stabilizer circuits being used), they are insufficient for exact tomography for general N [39, 40]. Regardless, \mathcal{C} can classically verify r in $\text{polylog } N$ time by checking $\gcd(p, N) = p \in \mathbb{P}$ [9].

The full multi-round protocol to factorize N blindly is as follows. \mathcal{C} runs consecutive rounds until either the correct period is obtained or any server dishonesty is flagged. In each round, she randomly executes one of the four RUV subprotocols. Specifically, she executes the computational subprotocol with some small probability η and the three security subprotocols (one CHSH and two tomography subprotocols) with probability $(1-\eta)/3$ each. The optimal choice of η is the sweet spot of factorizing successfully traded against detecting server malfeasance and, in practice, would be obtained by trial and error.